Application of a Reynolds stress model to separating boundary layers

By S. H. Ko

1. Motivation and objectives

Separating turbulent boundary layers occur in many practical engineering applications, yet the physics of separation/reattachment of the flows is poorly understood. During the past decade, various turbulence models have been proposed and their ability to successfully predict some types of flows has been shown. However, prediction of separating/reattaching flows is still a formidable task for model developers.

The present study is concerned with separation process from a smooth surface. Features of turbulent separating boundary layers that are relevant to modeling include: the occurrence of zero wall shear stress, which causes breakdown of the boundary layer approximation; the law of the wall not being satisfied in the mean backflow region; high turbulence levels in the separated region (Simpson *et al.* 1981); a significant low-frequency motion in the separation bubble (Dianat & Castro 1991); and the turbulence structure of the separated shear layer being quite different from that of either mixing layers or boundary layers (Dianat & Castro 1991). These special characteristics of separating boundary layers make it difficult for simple turbulence models to correctly predict their behavior.

Some researchers (De Henau *et al.* 1990, Atkinson & Castro 1991) have reported poor performance of existing turbulence models when the models were applied to the Simpson *et al.* (1981) separated flow experiment. They have found that a Reynolds stress model similar to Launder *et al.* (1975) and the standard k-ϵ model gave no separation — they could achieve separation only after an arbitrary increase of a coefficient in the ϵ equation. Menter (1991) evaluated various turbulence models ranging from algebraic to two-equation turbulence models for the marginal separated flow experiment of Driver (1991). He found that most mixing length models performed poorly, except for the Johnson-King model, and that the $k-\omega$ model predicted too high Reynolds shear stress.

An elliptic relaxation model, the $k-\epsilon-v$ model, was proposed by Durbin (1991) to treat the strongly non-homogeneous and anisotropic near-wall layer. This model eliminates the need for semi-empirical wall functions or *ad hoc* damping functions. Those functions assume universality of the near-wall flow, which is unwarranted in strongly adverse pressure gradients. After showing that the elliptic relaxation approach was successful in simple flows such as channel flow and flat plate, attached boundary layers, the model was extended to a full Reynolds stress model (RSM) (Durbin 1992) for more complicated near-wall problems. The primary objective of the present study is to apply the $k-\epsilon-v$ model and the full RSM to two-dimensional turbulent separating boundary layers.

2. Accomplishments

2.1 Turbulence model

The governing equations of the $k-\epsilon-v$ model can be found in last year's report (Ko, 1991). This section concerns only the equations of the RSM. The major difference between the $k-\epsilon-v$ model and the RSM is that the $k-\epsilon-v$ model uses an algebraic eddy viscosity expression, whereas the RSM uses differential equations for calculating Reynolds stresses in the time-averaged Navier-Stokes equations. It also has to be noted that the $k-\epsilon-v$ model can only be applied to thin shear layers while the RSM can be used for any complex flows.

The Reynolds stress transport equation is

$$\frac{D\overline{u_iu_j}}{Dt} = \mathcal{P}_{ij} + F_{ij} - \frac{\overline{u_iu_j}}{k}\epsilon + \frac{\partial}{\partial x_m}\left[(\nu + \frac{\nu_{ml}}{\sigma_k})\frac{\partial \overline{u_iu_j}}{\partial x_l}\right] \tag{1}$$

where

$$\mathcal{P}_{ij} = -\left(\overline{u_iu_k}\frac{\partial U_j}{\partial x_k} + \overline{u_ju_k}\frac{\partial U_i}{\partial x_k}\right) \tag{2}$$

is the rate of turbulence production by mean velocity gradients. In Eq. (1), the triple velocity correlation is modeled by the simple gradient-diffusion hypothesis of Daly & Harlow (1970):

$$\frac{\partial}{\partial x_m}(-\overline{u_mu_iu_j}) = \frac{\partial}{\partial x_m}\left(\frac{\nu_{ml}}{\sigma_k}\frac{\partial \overline{u_iu_j}}{\partial x_l}\right). \tag{3}$$

The tensorial eddy viscosity in Eq. (3) is

$$\nu_{ml} = C_\mu \overline{u_mu_l}\, T \tag{4}$$

where the time-scale T is

$$T = \max\left(\frac{k}{\epsilon}, C_T\left(\frac{\nu}{\epsilon}\right)^{1/2}\right). \tag{5}$$

The second term in Eq. (5) introduces the Komogorov time-scale as a lower bound.

The term F_{ij} in Eq. (1) includes the rest of the unclosed terms such as pressure gradient-velocity correlations and anisotropic dissipation ϵ_{ij}:

$$F_{ij} = -\frac{1}{\rho}\left(\overline{u_i\frac{\partial p}{\partial x_j}} + \overline{u_j\frac{\partial p}{\partial x_i}}\right) - \epsilon_{ij} + \frac{\overline{u_iu_j}}{k}\epsilon. \tag{6}$$

The elliptic relaxation model (Durbin 1992) for F_{ij} is

$$F_{ij} = k f_{ij} \tag{7}$$

$$L^2\nabla^2 f_{ij} - f_{ij} = \frac{(C_1-1)}{T}\left(\frac{\overline{u_iu_j}}{k} - \frac{2}{3}\delta_{ij}\right) + \frac{C_2}{k}\left(\mathcal{P}_{ij} - \frac{2}{3}\mathcal{P}\delta_{ij}\right) \tag{8}$$

where the length-scale L in Eq. (8) is expressed as

$$L = C_L \max\left(\frac{k^{3/2}}{\epsilon}, C_\eta\left(\frac{\nu^3}{\epsilon}\right)^{1/4}\right) \tag{9}$$

and $\mathcal{P} \equiv \mathcal{P}_{ii}/2$. The right side of Eq. (8) is simply the 'basic' model of Launder *et al.* (1975). Any other quasi-homogeneous Reynolds stress model could be used as the source term in this equation. Thus, the elliptic relaxation formulation primarily provides a framework for extending a quasi-homogeneous model to a model for near-wall turbulence.

The above RSM equations are coupled with transport equations for turbulent kinetic energy k and its rate of dissipation ϵ:

$$\underbrace{\frac{Dk}{Dt}}_{advection} = \underbrace{\mathcal{P}}_{production} \underbrace{-\epsilon}_{dissipation} + \underbrace{\frac{\partial}{\partial x_m}\left\{\left(\nu + \frac{\nu_{ml}}{\sigma_k}\right)\frac{\partial k}{\partial x_l}\right\}}_{diffusion} \tag{10}$$

$$\frac{D\epsilon}{Dt} = C_{\epsilon 1}\left(1 + 0.1\frac{\mathcal{P}}{\epsilon}\right)\frac{\mathcal{P}}{T} - C_{\epsilon 2}\frac{\epsilon}{T} + \frac{\partial}{\partial x_m}\left\{\left(\nu + \frac{\nu_{ml}}{\sigma_\epsilon}\right)\frac{\partial \epsilon}{\partial x_l}\right\}. \tag{11}$$

The model coefficients in Eqs. (4-11) are as follows

C_μ	C_T	C_1	C_2	C_L	C_η	$C_{\epsilon 1}$	$C_{\epsilon 2}$	σ_k	σ_ϵ
0.23	6.0	1.22	0.6	0.2	80.0	1.44	1.9	1.2	1.65

Detailed discussion of the RSM and its boundary conditions can be found in Durbin (1992).

2.2 Computational method

The $k - \epsilon - v$ model and the RSM were implemented into a finite difference computer code developed for solving 2-D, incompressible, steady-state turbulent flows. This program is based on finite difference procedures used in the TEACH computer program of Gosman and Pun (1974). The primitive variable equations are solved on a system of staggered grids. The discretization is based in all cases on the control volume approach.

The convective derivatives are approximated by the QUICK differencing scheme of Leonard (1979) in order to reduce the error due to the artificial viscosity. An iterative method for solving the algebraic finite-difference equations is employed. The SIMPLER algorithm of Patankar (1980) is used to obtain the pressure field from the continuity and momentum equations. The discretized equations are linear and are solved line-by-line using a tri-diagonal matrix algorithm applied in an alternating direction implicit manner. The accuracy of the present numerical methods has been tested by computing laminar flow in a driven cavity and laminar flow over a backward-facing step (Ko 1991).

2.3 Computation of separating boundary layer

The massive separating boundary layer of Simpson *et al.* (1981) was chosen as a test case. This flow is a two-dimensional, airfoil-type flow which was accelerated in a contraction and then decelerated until separation. It should be noted that the experimental data ended well before reattachment because the flow became increasingly three-dimensional downstream of separation.

Computations will be compared with experimental data for turbulence quantities as well as for the mean flow. The rectangular computational domain starts at the throat ($x = 1.6\,m$) of the wind tunnel where the flow is assumed to be a zero pressure gradient boundary layer. Reynolds number based on the momentum thickness and the free-stream velocity is 2800 at the inlet of the domain. A solution for a zero pressure gradient boundary layer is utilized to specify inlet conditions. The exit of the domain is located at $x = 8.6\,m$ which is sufficiently far downstream to permit reattachment of the flow and to allow zero-normal-gradient outflow conditions for all variables. In the vertical direction, the domain extends from the bottom wall to $y = 0.5\,m$.

Along the top boundary, the normal velocity V was specified to produce appropriate pressure gradients and the flow is assumed to be irrotational: $\partial U/\partial y = \partial V/\partial x$. A zero normal-gradient condition was applied to the other variables. On the solid wall, flow variables are specified as follows :

$$U = V = k = \overline{u_1{}^2} = \overline{u_2{}^2} = \overline{u_1 u_2} = f_{11} = 0,$$

$$\frac{d\overline{u_1{}^2}}{dy} = \frac{dk}{dy} = 0, \qquad \overline{u_2{}^2} = O(y^4), \qquad \overline{u_1 u_2} = O(y^4)$$

After grid independence testing, an 80 × 120 grid was selected for final computations. This had 80 uniformly-spaced lines in the streamwise direction and 120 uniformly-expanding lines in the transverse direction.

The prescribed V distribution at the top boundary is displayed in figure 1 along with the computed surface pressure coefficient, C_p. The inlet free-stream velocity U_{∞_0} ($= 21.7\ m/s$) was used to normalize the V velocity. Since the V profile at the top boundary could not be obtained from the experimental data, it was selected by matching the U-velocity of the experiments at the 99% boundary layer thickness. The experimental data only cover the region $x < 4.34\ m$. The V distribution downstream of this was arbitrarily chosen to close the separation bubble. Regrettably, this arbitrariness, stemming from the incompleteness of the data, makes the present comparison to experiment somewhat ambiguous. It should be mentioned that this V-profile matching was done only for computations of the $k-\epsilon-v$ model, and then the same V profile was used for computations of the RSM without adjustment. This adds additional ambiguity to the comparison of results of the RSM to experiment. The computed C_p profiles show good agreement with experimental data until the flow separates at $x = 3.45\ m$. In the separated region, the RSM overpredicts C_p whereas the $k-\epsilon-v$ model underpredicts C_p. Since C_p is a measure of the magnitude of mean velocity in the near-wall region, the C_p profiles in the figure could

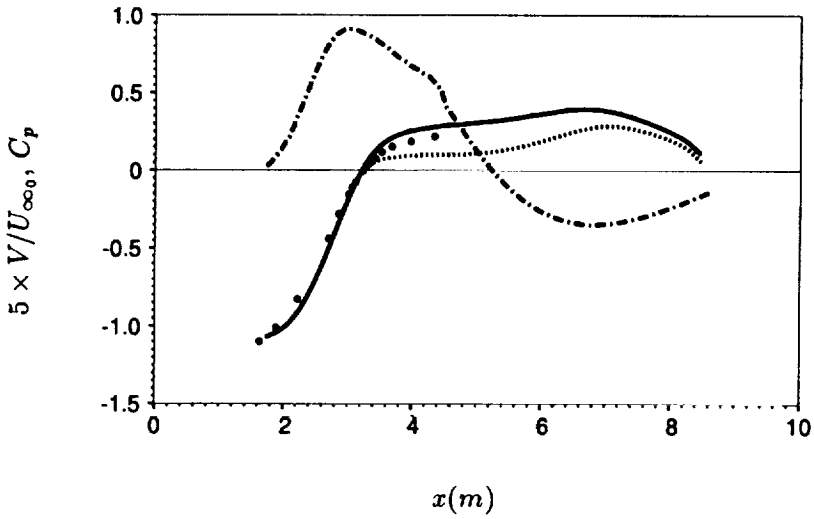

FIGURE 1. Prescribed V distribution at top of computational domain (—·—) and surface pressure coefficient C_p computed by the RSM (———) and the $k-\epsilon-v$ model (·····). • data (Simpson *et al.* 1981).

be interpreted as follows: the separation predicted by the RSM is weaker than that predicted by the $k-\epsilon-v$ model.

Figure 2 shows the computed streamline patterns and the computational domain. As suggested by figure 1, the $k-\epsilon-v$ model gives earlier separation and larger separation bubble compared to the RSM for the same V profile along the top boundary.

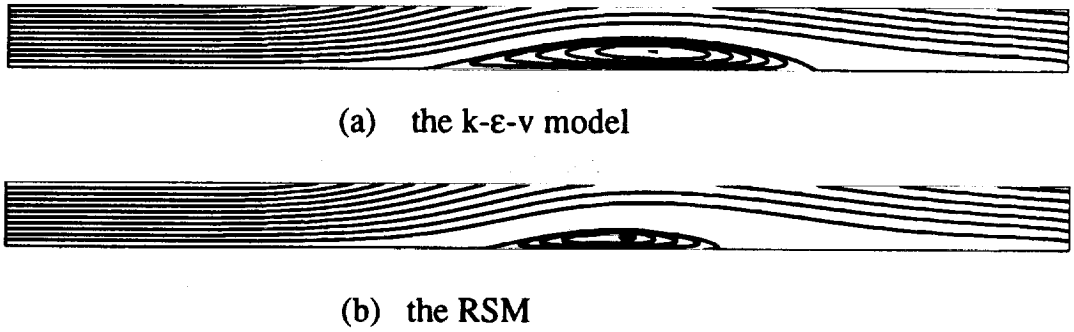

FIGURE 2. Predicted streamline patterns, showing computational domain.

Computed skin friction coefficients C_f are compared to measurements in figure 3. The agreement between model calculations and experimental results is reasonable in the region upstream of separation. In the separation region, the two models show

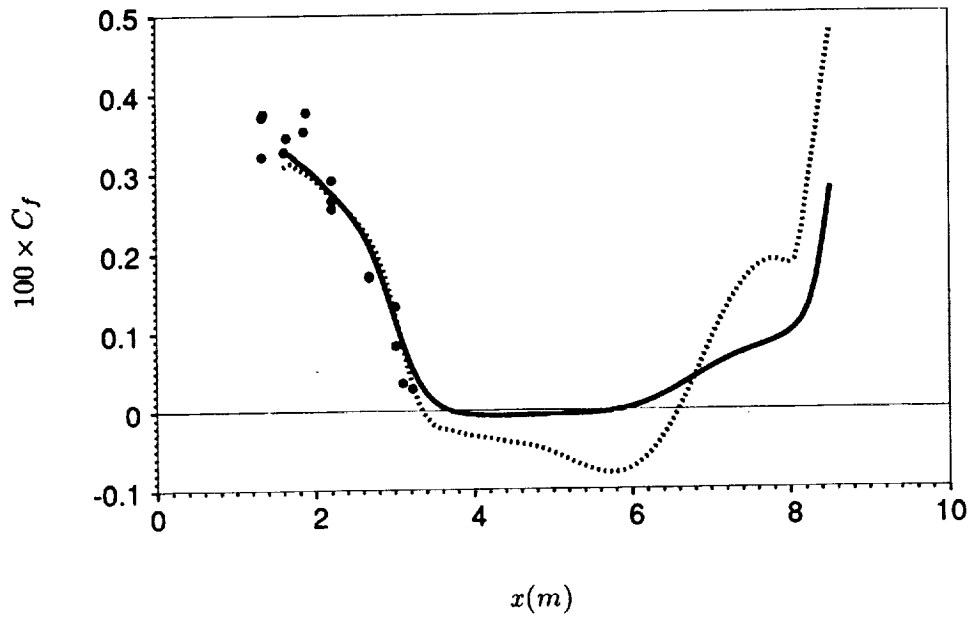

FIGURE 3. Skin friction coefficient C_f computed by the RSM (———) and the $k - \epsilon - v$ model (·····). • data (Simpson *et al.* 1981).

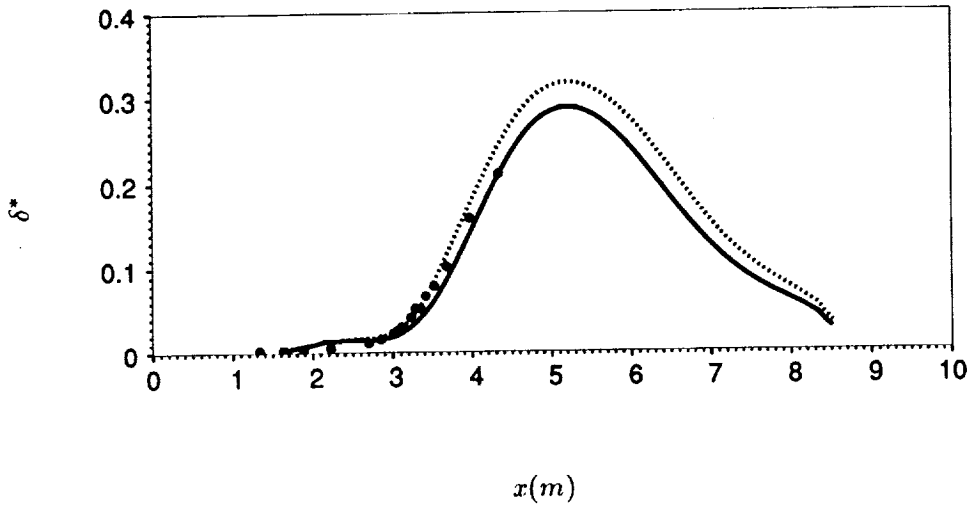

FIGURE 4. Displacement thickness δ^* computed by the RSM (———) and the $k - \epsilon - v$ model (·····). • data (Simpson *et al.* 1981).

a substantial difference; this is expected from the previous figures. The computed C_f's become negative at $x = 3.72\,m$ for the RSM and at $x = 3.35\,m$ for the $k - \epsilon - v$ model, while the measured separation was at $x = 3.45\,m$. However, this discrepancy is not very significant because of the ambiguity in prescribing V, alluded to previously. Celenligil & Mellor (1985) found that their results were very sensitive to the prescribed external pressure gradient. Figure 4 shows a reasonable agreement between the computed displacement thickness δ^* and measurements. It should be noted that as the flow separates, the δ^* grows drastically due to the reverse flow in the separated region. Once again, the $k - \epsilon - v$ model shows stronger displacement effects than the RSM in the separated region. Figures 5 – 9 show more detailed results. In these figures, the x-coordinate is measured relative to the separation point, which is equated to the experimental value of $3.45\,m$. In this way, comparison at various positions will give fair insight on how the model solutions evolve in space upstream and downstream of separation.

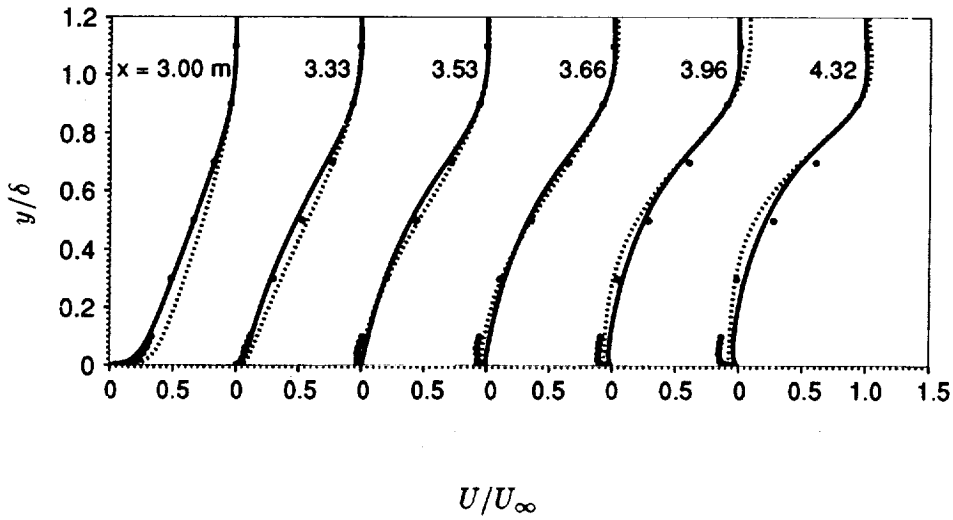

FIGURE 5. Mean flow profiles upstream and in the separated region. • data (Simpson *et al.* 1981).

Figure 5 shows the x-component of the mean velocity at various positions upstream and within the separated region. In the separated region, the $k - \epsilon - v$ model calculation shows closer agreement with measurements than the RSM calculation. However, this is mainly because the V profile along the top boundary was obtained for the $k - \epsilon - v$ model. Generally, the models predict the U-velocity profiles in the outer region reasonably well, but they underpredict mean backflow in the separated region. This underprediction of backflow is probably due to the Reynolds stress gradient being too large near the wall, hence transferring too much forward momentum from the outer flow.

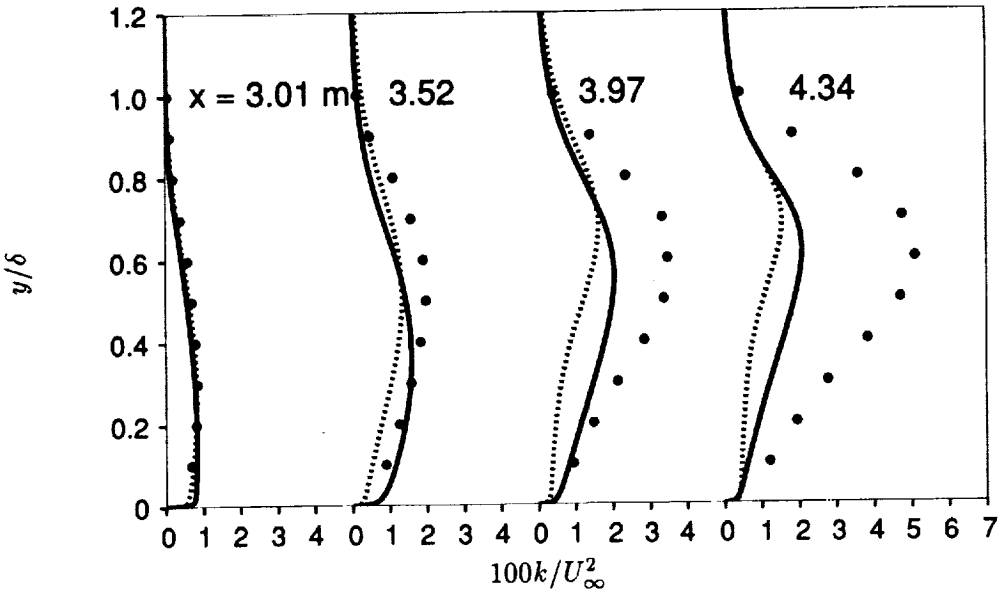

FIGURE 6. Profiles of turbulent kinetic energy computed by the RSM (——) and the $k-\epsilon-v$ model (·····). • data (Simpson *et al.* 1981).

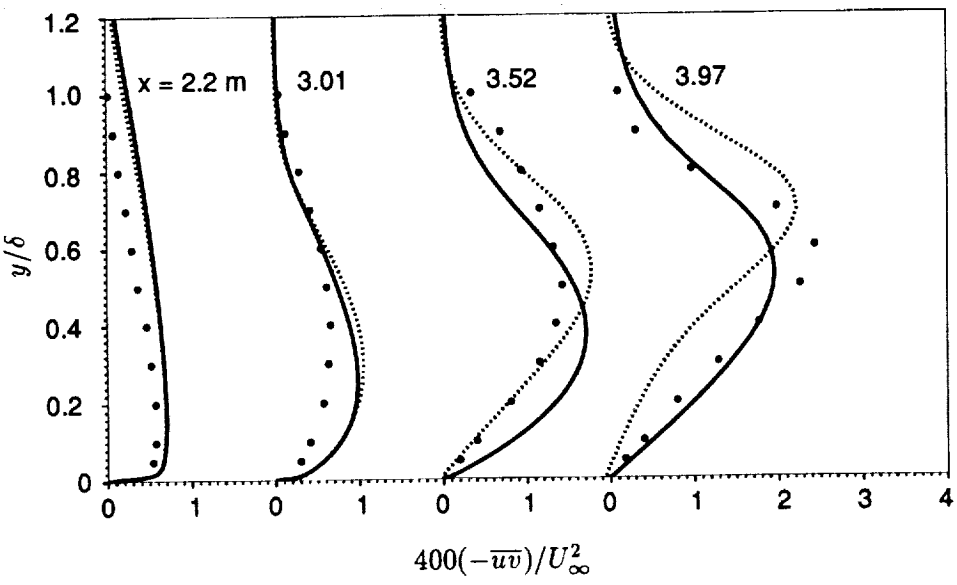

FIGURE 7. Profiles of Reynolds shear stress computed by the RSM (——) and the $k-\epsilon-v$ model (·····). • data (Simpson *et al.* 1981).

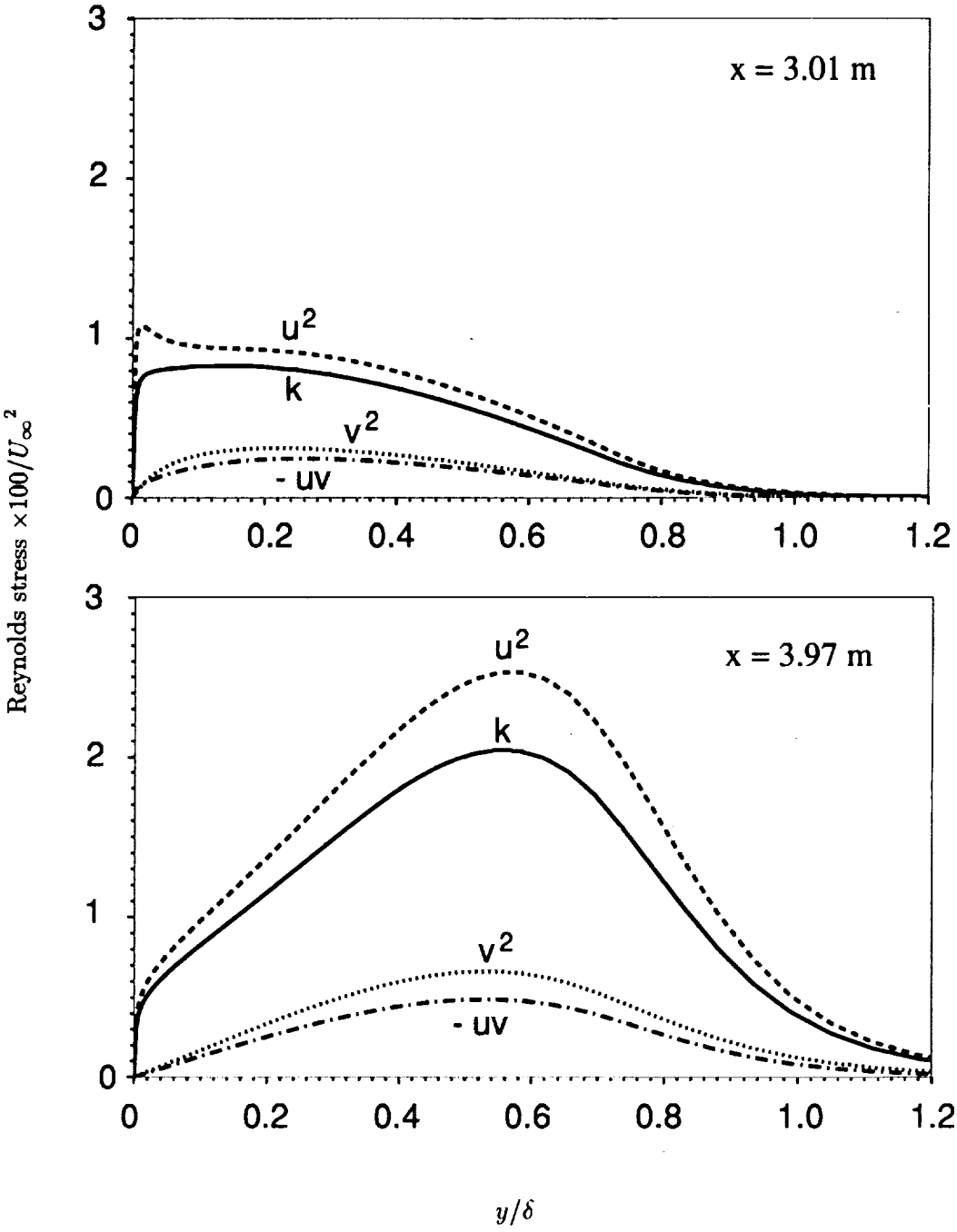

FIGURE 8. Profiles of Reynolds stresses.

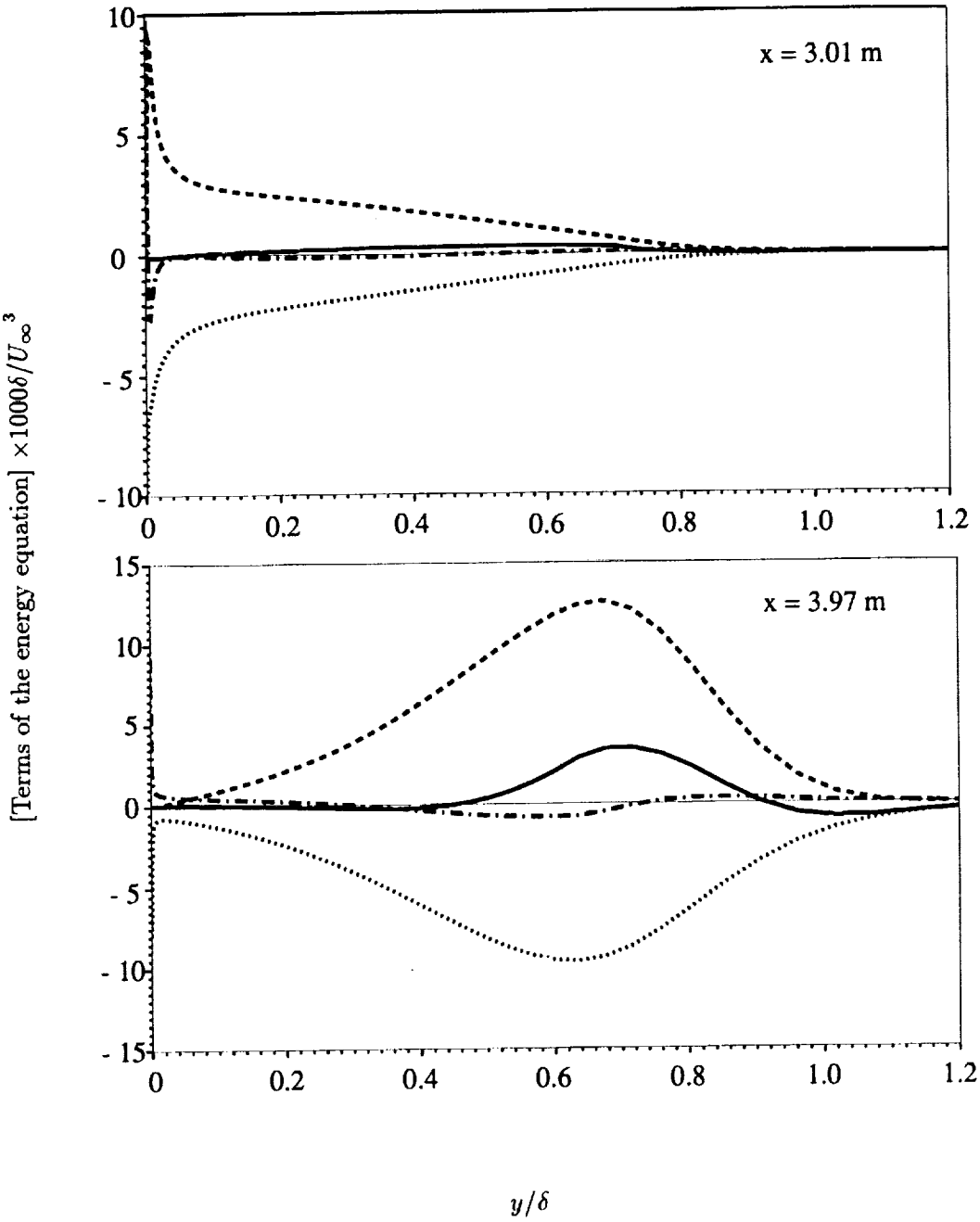

FIGURE 9. Turbulence energy balance : ——— , advection; - - - - , production; ····· , dissipation; —·— , diffusion.

Figures 6 and 7 show turbulent kinetic energy and Reynolds shear stress profiles at various positions. The turbulent kinetic energy predictions by both the $k-\epsilon-v$ model and the RSM are significantly too low in the separated shear layer. Low predictions of k were similarly found by De Henau *et al.* (1990) and Atkinson & Castro (1991). In figure 7, the level of $-\overline{uv}$ is in general agreement with experiments, but discrepancies exist in the shapes of the profiles. The models of Celenligil & Mellor (1985) and Atkinson & Castro (1991) severely underpredicted the Reynolds shear stress in the separated region.

In figure 8, profiles of Reynolds stresses computed by the RSM are plotted at $x = 3.01\,m$, and $3.97\,m$ upstream and downstream of the separation, respectively. As expected, Reynolds stresses at $x = 3.01\,m$ have profiles typical of an adverse-pressure-gradient boundary layer. At $x = 3.97\,m$ the maxima of Reynolds stresses occur at $y/\delta \approx 0.55$. Profiles of $\overline{w^2}$ can be deduced from the figure using the relationship $\overline{w^2} = 2k - (\overline{u^2} + \overline{v^2})$, which yields $\overline{w^2} \approx \overline{v^2}$ over a wide range. Overall, one can say that $\overline{u^2}$ is the largest and $\overline{uv}$ is the smallest of Reynolds stress components everywhere.

Figure 9 shows balances of the turbulence kinetic energy equation. Terms in Eq. (10) were normalized by the boundary layer thickness and local free-stream velocity. The production is mainly balanced by the dissipation while the advection and the diffusion are relatively small.

In conclusion, predictions of skin friction and displacement thickness for the pressure-induced separating boundary layer are in agreement with experimental measurements, but both the $k-\epsilon-v$ model and the RSM show insufficient back-flow in the separated region. The models also underestimate the turbulent kinetic energy in the separated shear layer; the Reynolds shear stress is more accurately predicted. Overall, the separated flow computation was a bit unsatisfactory because suction and blowing at the upper boundary had to be imposed to simulate the experimental conditions. However, it is significant that the $k-\epsilon-v$ model and the RSM are able to produce a reasonable separated flow.

3. Future plans

Further assessment and improvement of the RSM for separated flows will continue in the future. Due to the ambiguity of the imposed flow conditions for the pressure-driven separated boundary layer computation, it is difficult to draw any conclusion on the model performance. Therefore, it is necessary to have a well-defined test case with clear-cut boundary conditions in order to isolate phenomena which are directly related to the turbulence model. With this consideration, turbulent flow over a backward-facing step is chosen as the next test case. The backward-facing step flow is an excellent case not only for studying the flow physics of separated and reattaching turbulent shear layers, but also for developing turbulence models. Numerical results will be compared with DNS (Direct Numerical Simulation) as well as experimental data.

As discussed in §2.1, a possible model improvement can be achieved simply by substituting a new quasi-homogeneous Reynolds stress model for the source term

in Eq. (8). The present RSM uses the basic version of the LRR model (Launder *et al.* 1975) in which the modeled rapid pressure-strain correlation is linear in the anisotropy tensor. Following the LRR model, many new ideas have been employed to develop more elaborate models for the last decade. Recently, Speziale *et al.* (1991) introduced a new second-order closure model - the SSG model - which is based on invariant dynamical systems analysis coupled with some additional constrains. This model is quadratically nonlinear in the anisotropy tensor and shows improvement over the LRR model for a variety of homogeneous turbulent flows. After investigating the performance of the RSM for the backward-facing step flow, the feasibility of the SSG model as the source term for the elliptic relaxation formulation will be studied.

REFERENCES

ATKINSON, K. N. & CASTRO, I. P. 1991 Computations of a separated turbulent boundary layer, Turbulent Shear Flows Conference, 20-2.

CELENLIGIL, M. C.& MELLOR, G. L. 1985 Numerical solution of two-dimensional turbulent separated flows using a Reynolds stress closure model. *J. Fluids Engr.* **107,** 467-476.

DALY, B. J. & HARLOW, F. H. 1970 Transport equations of turbulence. *Phys. Fluids.* **13,** 2634-2649.

DE HENAU, V., RAITHBY, G. D. & THOMPSON, B. E. 1990 Prediction of flows with strong curvature and pressure gradient using the k-ϵ turbulence model. *J. Fluids Engr.* **112,** 40-47.

DIANAT, M. & CASTRO, I. P. 1991 Turbulence in a separated boundary layer. *J. Fluid Mech.* **226,** 91-123.

DRIVER, D. M. 1991 Reynolds shear stress measurements in a separated boundary layer flow, AIAA paper 91-1787.

DURBIN, P. A. 1991 Near-wall turbulence closure modeling without "damping functions". *Theoretical and Computational Fluid Dynamics.* **3,** 1-13.

DURBIN, P. A. 1992 Near wall turbulence closure modeling without 'damping functions'. *CTR Manuscript 113,* Stanford Univ./NASA Ames (to appear in *J. Fluid Mech.*).

GOSMAN, A. D.& PUN, W. M. 1974 Calculation of recirculating flows. Research Report No. HTS/74/2., Dept. Mech. Engr. Imperial College, London, England.

KO, S. 1991 Near-wall turbulence modeling for boundary layers with separation. *Annual Research Briefs.* Center for Turbulence Research, Stanford Univ./NASA Ames, 137-146.

LAUNDER, B. E., REECE, G. J. & RODI, W. 1975 Progress in the development of a Reynolds-stress turbulence closure. *J. Fluid Mech.* **68,** 537-566.

LEONARD, B. P. 1979 A stable and accurate convective modelling procedure based on quadratic upstream interpolation. *Computer Methods in Applied Mechanics and Engr.* **19,** 59-98.

MENTER, F. R. Performance of popular turbulence models for attached and separated adverse pressure gradient flows, AIAA paper 91-1784.

PATANKAR, S. V. 1980 Numerical Heat Transfer and Fluid Flow. McGraw-Hill, New York.

SIMPSON, R. L., CHEW, Y. -T. & SHIVAPRASAD, B. G. 1981 The structure of a separating turbulent boundary layer. Part 1. Mean flow and Reynolds stresses. *J. Fluid Mech.* **113,** 23-51.

SPEZIALE, C. G., SARKAR, S.& GATSKI, T.B. 1991 Modelling the pressure-strain correlation of turbulence: an invariant dynamical systems approach. *J. Fluid Mech.* **277,** 245-272.